Yuki Ideguchi*, Kenji Kamimura, Koji Kimura,
Shinya Hosokawa, Naohisa Happo, Kouichi Hayashi,
Yoshihiro Ebisu, Toru Ozaki, Jens R. Stellhorn, Motohiro Suzuki,
Hiroyuki Okazaki, Aichi Yamashita, and Yoshihiko Takano

X-ray Fluorescence Holographic Study on High-Temperature Superconductor $FeSe_{0.4}Te_{0.6}$

Abstract: To observe the difference of atomic heights between the Se and Te layers with respect to the Fe layer in $FeSe_{0.4}Te_{0.6}$ single crystal, a Fe $K\alpha$ fluorescence X-ray holography (XFH) experiment was performed at room temperature. The crystal structure of superconductor $FeSe_{0.4}Te_{0.6}$ obtained by X-ray diffraction (XRD) at a low temperature has distinct z-coordinates of Se and Te, remarkably different from each other. The reconstructed atomic image around central Fe atoms by XFH, however, reveals the different and complex results.

Keywords: Superconductor, FeSeTe, X-ray Fluorescence Holography, Chalcogen Height, Local Atomic Structure, Positional Fluctuations, Atomic Image.

*Corresponding author: Yuki Ideguchi, Department of Physics, Graduate School of Science and Technology, Kumamoto University, Kumamoto 860-8555, Japan, e-mail: 152d8002@st.kumamoto-u.ac.jp
Kenji Kamimura, Koji Kimura, Shinya Hosokawa: Department of Physics, Graduate School of Science and Technology, Kumamoto University, Kumamoto 860-8555, Japan
Naohisa Happo: Graduate School of Information Sciences, Hiroshima City University, Hiroshima 731-3194, Japan
Kouichi Hayashi: Department of Materials Science and Engineering, Graduate School of Engineering, Nagoya Institute of Technology, Nagoya 466-8555, Japan
Yoshihiro Ebisu, Toru Ozaki: Research Center for Condensed Matter Physics, Hiroshima Institute of Technology, Hiroshima 731-5193, Japan
Jens R. Stellhorn: Department of Chemistry, Physical Chemistry, Philipps University of Marburg, 35032 Marburg, Germany
Motohiro Suzuki: Japan Synchrotron Radiation Research Institute (JASRI), SPring-8, Sayo, Hyogo 679-5198, Japan
Hiroyuki Okazaki, Aichi Yamashita, Yoshihiko Takano: National Institute for Materials Science, Tsukuba 305-0047, Japan
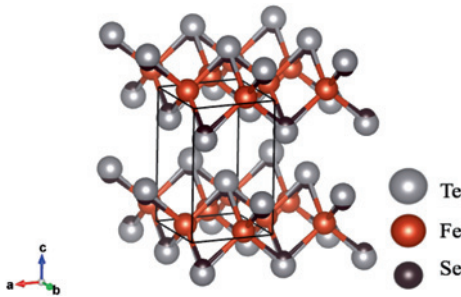
Figure 1: Layer structure in the $FeSe_{0.4}Te_{0.6}$ tetragonal crystal [2]. Balls indicate Te, and Fe, and Se atoms.

Table 1: Atom position in $FeSe_{0.4}Te_{0.6}$ single crystal obtained by XRD [1].

Atoms	Occupancy	x	y	z
Fe	1	$\frac{3}{4}$	$\frac{1}{4}$	0
Se	0.4	$\frac{1}{4}$	$\frac{1}{4}$	0.2468(7)
Te	0.6	$\frac{1}{4}$	$\frac{1}{4}$	0.2868(3)

1 Introduction

$FeSe_xTe_{1-x}$ is one of the simplest Fe-based superconductors, and has intensively been studied concerning the interplay between structural or magnetic degrees of freedom and superconductivity. It is widely accepted that magnetic fluctuations play a very important role for their superconducting nature.

Figure 1 shows the crystal structure of $FeSe_xTe_{1-x}$ determined by XRD (space group $P4/nmm$, lattice constant a = 3.7996 Å, c = 5.9895 Å) [1]. The crystal structure of $FeSe_xTe_{1-x}$ is an isovalent substitution of Te for Se in FeSe. Since Se and Te have quite different ionic radii: r_{Se} = 1.98 Å and r_{Te} = 2.21 Å, respectively [2], they have different z-coordinates as shown in Table 1 [1]. A density functional calculation study revealed a strong sensitivity of the magnetic moment to the chalcogen heights, i.e., the distances of the Se/Te layers from the Fe plane [3].

Fe-based superconductors show differential superconducting properties by the various pressure effects [4]. T_c of almost Fe based superconductors included FeSe under high pressure show higher T_c than those under the ambient pressure, and anion height dependence of T_c shows symmetric curve with a peak around 1.38 Å. It agrees with the unique curve for not only ambient pressure but also under high pressure. However, $FeSe_{0.4}Te_{0.6}$ does not obey this curve, and the anion height of $FeSe_{0.4}Te_{0.6}$ under high pressure is much higher than that expected from the unique curve. One of the obvious differences between FeSe and $FeSe_{0.4}Te_{0.6}$

is whether the disorder exists at the anion site or not. If T_c of the Fe-based superconductor strongly depends on the anion height, the disorder at the anion site should strongly affect the superconducting properties of the Fe-based superconductor. Thus, to observe the local disorder at the anion site is required for the further understanding of superconductivity.

To examine the validity of the XRD result, a different technique is necessary to precisely obtain the local structure around the Fe atoms. The X-ray fluorescence holography (XFH) is a newly developed technique that enables one to draw three-dimensional (3D) atomic images around a specific element emitting fluorescent X-rays [5]. Due to the interference between the direct incident X-rays and those scattered by the surrounding atoms, the fluorescent X-ray intensity from the emitter slightly modulates with the incident X-ray angles by about 0.1%, from which 3D images can be obtained by simple Fourier transforms without any special models. We have performed Fe $K\alpha$ XFH measurements on an FeSe$_{0.4}$Te$_{0.6}$ single crystal at room temperature. In this paper, we report atomic images of Se and Te around the central Fe atom and discuss the different roles of the Se and Te atoms for the superconducting nature in the crystal.

2 Experimental procedure

A single crystal of FeSe$_{0.4}$Te$_{0.6}$ superconductor was grown using a slow-cooling method from its melt. In the slow-cooling method, FeSe$_{0.4}$Te$_{0.6}$ polycrystal was placed in a BN crucible sealed in an Ar-filled Mo capsule. It was then heated to 1150 °C, followed by cooling to 780 °C for 80 h, and then cooled to room temperature. The crystal was cut and polished so as to have a (001) flat surface larger than 3×3 mm^2. The crystalinity of the sample was examined by taking a Laue photograph, and the concentration and homogeneity over the sample were confirmed within the experimental errors by an electron-probe micro-analysis.

XFH measurements were carried out at the beamline BL39XU in the SPring-8, Hyogo, Japan. Figure 2 shows a schematic diagram of the XFH experiment. The sample was placed on a two-axes table of a diffractometer installed at the beamline. The measurements were performed in inverse mode by rotating two axes, the exit angle of $0° \leq \theta \leq 75°$ in steps of $1.00°$, and the azimuthal angle of $0° \leq \varphi \leq 360°$ in steps of about $0.3°$, of the sample stage. Incident X-rays were focused onto the (001) surface of the sample. Fe $K\alpha$ fluorescence X-rays were collected using an avalanche photodiode detector with a toroidal graphite crystal energy-analyzer. The XFH signals were recorded at eight different incident X-ray energies from 7.5
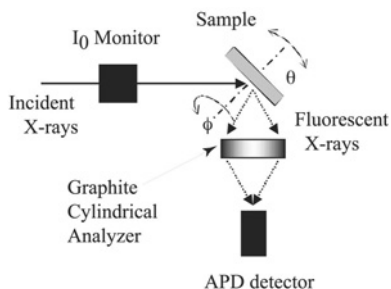
Figure 2: Schematic diagram of the XFH equipment.

to 11.0 keV in steps of 0.5 keV. Each scan took about 3 h. Details of the XFH experimental technique are given elsewhere [5].

    Holographic oscillation data were obtained by subtracting the background from the fluorescent X-ray intensities and by normalizing them to the incident X-ray intensities. An extension of the hologram data was carried out using the crystal symmetry of the tetragonal structure and the measured X-ray standing wave lines, using a twofold rotational symmetry around the $\langle 001 \rangle$ direction and a mirror symmetry with the (110) plane. From the holographic patterns, 3D atomic configuration images were reconstructed using Barton's algorithm [6] by superimposing the holograms with eight different incident X-ray energies, which can highly suppress the appearance of twin images. Details of the data analysis are given elsewhere [7].

3 Results and discussion

Figure 3 shows an example of the Fe $K\alpha$ hologram pattern of the $FeSe_{0.4}Te_{0.6}$ single crystal measured at an incident X-ray energy of 7.5 keV. The radial and angle directions indicate θ and φ, respectively, and the magnitudes are given as the color bar shown beside the figure. A twofold symmetry was observed in the holographic pattern, indicating a good quality of the sample crystal.

    Figure 4 shows the reconstructed atomic images of $FeSe_{0.4}Te_{0.6}$ single crystal on the (001) plane around the central Fe atom marked by a circle. The dashed lines indicate the boundary of unit cells obtained by XRD [1]. Fe atoms should be observed on intersections of dashed lines and the centers of the unit cell squares. As seen in Figure 4, the first-neighbor Fe atoms on this plane are observed at positions nearer than the center of squares around the central Fe atom. The second-neighbor Fe atoms on this plane are located at a distant position with respect to the intersections of the dashed lines. However, the third or more-distant Fe atoms
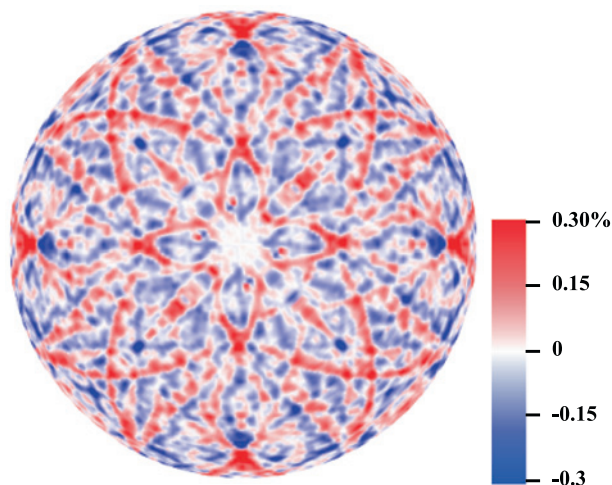
Figure 3: An example of Fe $K\alpha$ hologram pattern obtained from a (001) surface of the $FeSe_{0.4}Te_{0.6}$ single crystal measured at an incident X-ray energy of 7.5 keV.
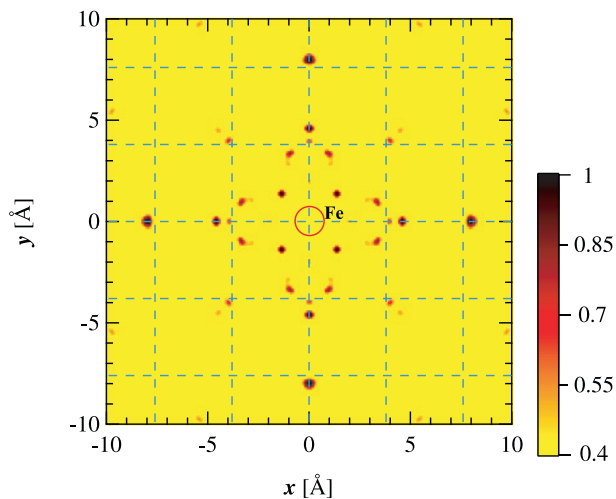

Figure 4: Atomic image of $FeSe_{0.4}Te_{0.6}$ single crystal on the (001) plane at $z = 0$ Å around the central Fe atom. Areas surrounded by dashed line indicate unit cells.

on this plane are observed mostly at or slightly distant from the appropriate positions, where slight differences in the atomic positions may be due to the temperature difference. As a result, the structural distortions of the Fe atoms are found to be limited within the second nearest neighbor.

The positions of the first-neighbor Fe atoms obtained from the present XFH do not coincide with those from the previous XRD data [2]. It is highly possible that images of the first-neighbor Fe atoms are largely deformed and shifted nearer due to the noises or artifacts of the present XFH data. Discrepancies in interatomic distances are sometimes found between diffraction and XFH (XAFS) data as dis-
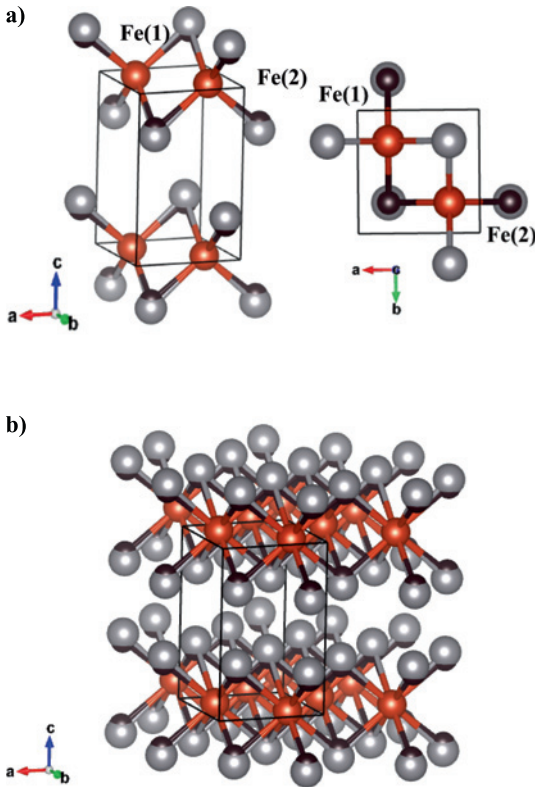
a)

b)

Figure 5: (a) Two-sites of the Fe atoms in the unit cell. Red balls indicate Fe atoms. (b) The crystal structure of $FeSe_{0.4}Te_{0.6}$ observable by XFH (space group *P4/nbm*).

cussed in our previous paper on GeTe crystal [8]. Namely, the diffraction detects an average (or gravity) of atomic distributions, while the XFH (XAFS) observes its peak position. If the atomic distribution is asymmetric, the average and peak positions are different, and a difference between interatomic distances obtained from diffraction and XFH is realized, which was confirmed by XAFS and ab initio molecular dynamics simulation for GeTe crystal [8]. Even though such shifts are taken into account, however, the present positional shifts seem to be too large. To determine the exact positions of the Fe neighbors, we plan to carry out XAFS measurement for the same sample.

As mentioned above, it should be carefully observed how the Se and Te atoms are located around the central Fe atoms in the crystal. For this, it should be understood that the Fe atoms have two different central sites in the unit cell, as shown Fe(1) and (2) in Figure 5(a). It is not possible to distinguish these two sites by the XFH measurement, and XFH can observe a mixture of atomic images from two different central Fe sites. Namely, the structure of $FeSe_{0.4}Te_{0.6}$ observed by XFH is not the original space group *P4/nmm*, but should be considered as the space
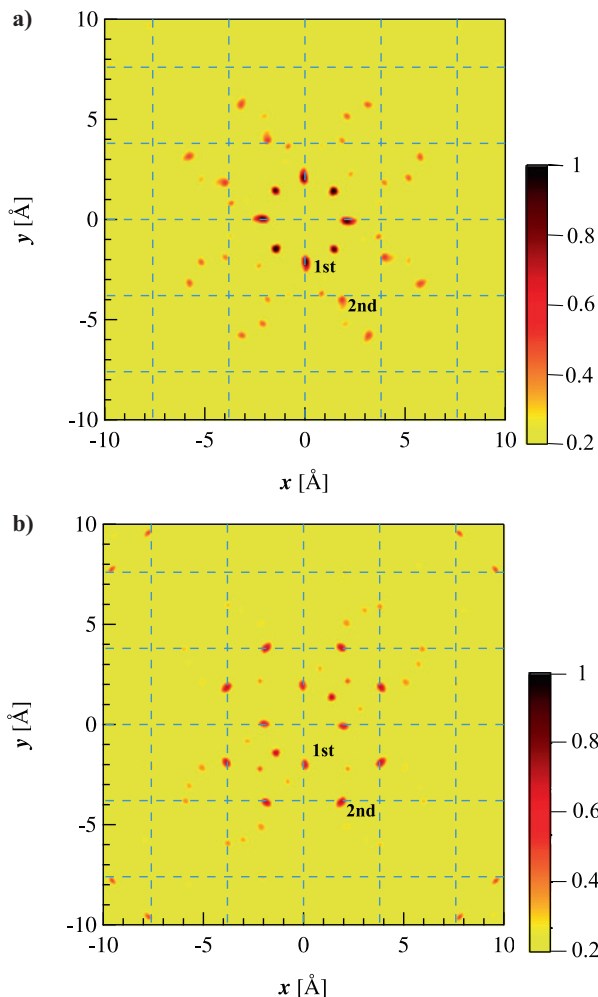
Figure 6: (a) An atomic image of the $FeSe_{0.4}Te_{0.6}$ single crystal on the (001) plane at the $z = 1.478\,Å$ (Se layer). (b) An atomic image of the $FeSe_{0.4}Te_{0.6}$ single crystal on the (001) plane at the $z = 1.718\,Å$ (Te layer).

group $P4/nbm$, as shown Figure 5(b). Note that atomic image intensities of Se and Te atoms should be a half of those produced using this figure.

Figures 6(a) and (b) show the reconstructed atomic images on the (001) planes at $z = 1.478$ Å (the height of the Se plane) and at $z = 1.718$ Å (that of the Te plane), respectively. The image intensities of these figures are normalized to the maximum value the Figure 6(a) for the comparison, and are shown as the color bars beside the figures. The image intensities of the first-neighbor Se/Te atoms as seen in Figure 6(a) are stronger than those in Figure 6(b), which is inconsistent with the XRD result, i.e., the Se images in Figure 6(a) should be weaker than the Te images in Figure 6(b), owing to the difference of X-ray scattering cross-sections between the
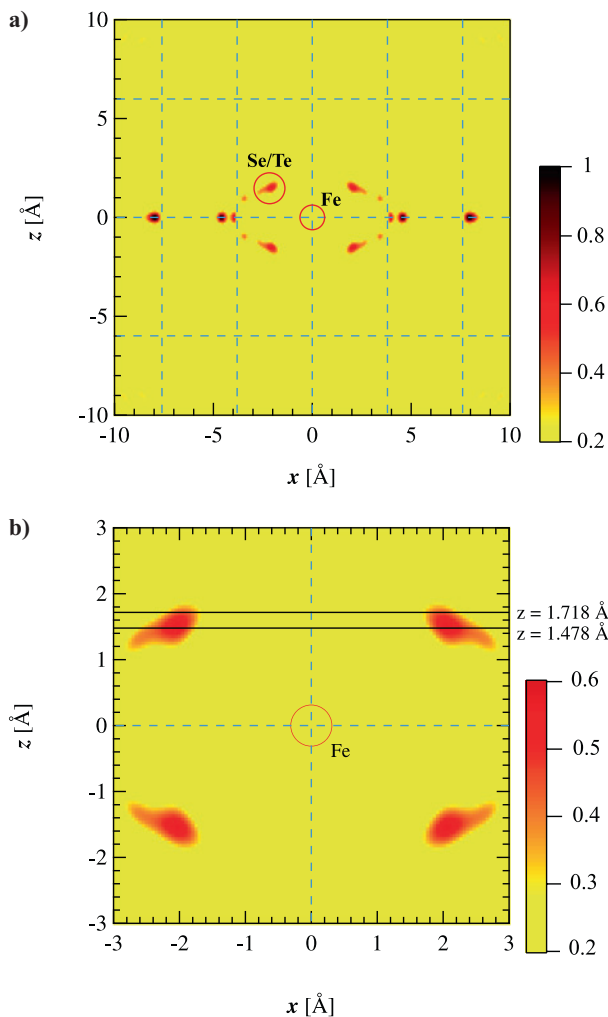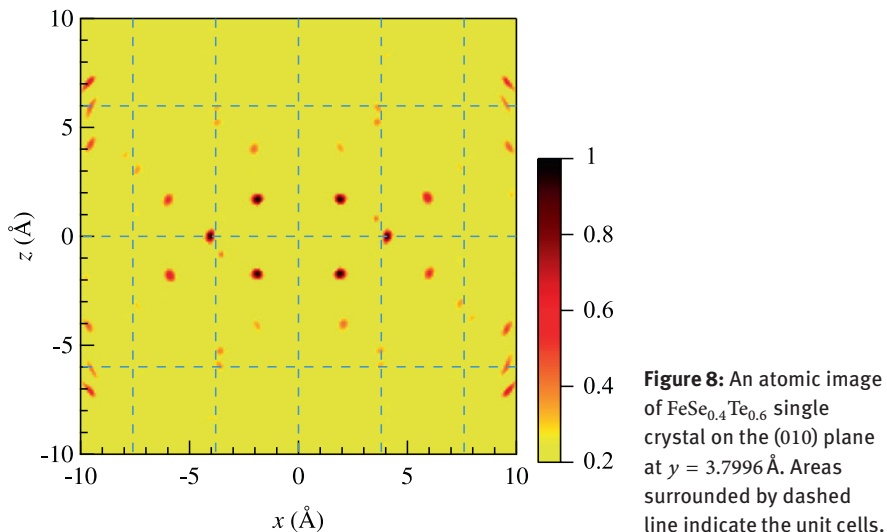
Figure 7: (a) An atomic image of $FeSe_{0.4}Te_{0.6}$ single crystal on the (010) plane at $y = 0$ Å. Areas surrounded by dashed lines indicate the unit cells. (b) An atomic image enlarged near the center of Figure 7(a) for the clarity.

Se and Te elements. In addition, first-neighbor Se/Te atoms in Figure 6(a) show elliptical atomic images along the radial direction as compared with those in Figure 6(b). These XFH results indicate that the positions of the Se/Te atoms are not simple unlike the XRD result, and positional fluctuations are observed along the radial directions. It is one of the excellent advantages of XFH that positional fluctuations of independent atoms can be observed as 3D images.

On the other hand, the image intensities of second-neighbor Se/Te atoms in Figure 6(b) are stronger than those in Figure 6(a), and located at mostly ideal po-

Figure 8: An atomic image of $FeSe_{0.4}Te_{0.6}$ single crystal on the (010) plane at $y = 3.7996\,\text{Å}$. Areas surrounded by dashed line indicate the unit cells.

sitions determined by XRD. From this, it is found that Te atoms can also be located at the height of the Se planes.

Figure 7(a) shows the reconstructed atomic images on the (010) plane around the central Fe atoms at $y = 0\,\text{Å}$, and Figure 7(b) shows an enlarged image of Figure 7(a) for a detailed observation. The solid lines in Figure 7(b) indicate the positions of the Se/Te layers. As mentioned above, the image intensity at $z = 1.478\,\text{Å}$ is stronger than that at $z = 1.718\,\text{Å}$. Because the concentration of Te atoms is larger than that of Se atoms in $FeSe_{0.4}Te_{0.6}$ single crystal if Te atoms locate at the position provided by XRD [1], the image intensity at $z = 1.718\,\text{Å}$ should be much stronger than that at $z = 1.478\,\text{Å}$. First-neighbor Se/Te atomic positions mainly fluctuate in the angular direction on the (010) plane, which was, in regard to appearance, observed in the radial direction on the (001) plane shown in Figure 6(a).

Figure 8 shows the reconstructed atomic imaged on the (010) plane at $y = 3.7996\,\text{Å}$. Namely, second-neighbor and third or more distant Se/Te atoms from central Fe atoms can be observed in this reconstructed image. In comparison with Figure 7, second-neighbor Se/Te atomic positions hardly fluctuate in the angular direction, and the maximum intensity point is $z = 1.7\,\text{Å}$, where agree with Te – Fe layer height provide XRD. So, Se/Te atoms seem to stable by the long-range order such XRD measurement, but those locally fluctuate in angular direction by short-range order such XFH measurement. This may be correlated with the higer anion height under high pressure.

The present XFH experiments at room temperature show interesting features on the local atomic structures, which are quite different from those expected from

the XRD measurement. For the further understandings of the interplay between structural and superconductivity in the $FeSe_{0.4}Te_{0.6}$ alloy, a detailed XFH experiment at low temperatures is essential, which is now in progress.

4 Conclusion

We have carried out a Fe $K\alpha$ fluorescence X-ray holography experiment on $FeSe_{0.4}Te_{0.6}$ single crystal. The reconstructed atomic images around the central Fe atom reveal that the local lattice constant is slightly larger than the lattice constant obtained by the XRD refinement. The difference of the chalcogen heights along the z-coordinate is not clearly observed. But, Se and Te atoms are observed to fluctuate along angular direction. To confirm the present findings, XAFS measurements should be carried out. For the further understandings of the interplay between structural and superconductivity in $FeSe_{0.4}Te_{0.6}$, an XFH experiment at low temperatures is essential.

References

1. M. Tegel, C. Löhnert, and D. Johrendt, Solid State Commun. **150** (2010) 383.
2. R. D. Shannon and C. T. Prewitt, Acta Crystallogr. **25** (1969) 925.
3. C.-Y. Moon and H. J. Choi, arXiv:0909.2916.
4. Y. Mizuguchi and Y. Takano, J. Phys. Soc. Jpn. **79** (2010) 102001.
5. K. Hayashi, N. Happo, S. Hosokawa, W. Hu, and T. Matsushita, J. Phys.-Condens. Mat. **24** (2012) 093201.
6. J. J. Barton, Phys. Rev. Lett. **67** (1991) 3106.
7. N. Happo, K. Hayashi, and S. Hosokawa, Jpn. J. Appl. Phys. **49**, (2010) 116601.
8. S. Hosokawa, N. Happo, S. Senba, T. Ozaki, T. Matsushita, A. Koura, F. Shimojo, and K. Hayashi, J. Phys. Soc. Jpn. **83** (2014) 124602.